Progress In Electromagnetics Research, Vol. 143, 47–66, 2013

GENERALIZED WAIT-HILL FORMULATION ANALYSIS OF LUMPED-ELEMENT PERIODICALLY-LOADED ORTHOGONAL WIRE GRID GENERIC FREQUENCY SELECTIVE SURFACES

Christos Mias[1, *] and Angelo Freni[2]

[1]School of Engineering, University of Warwick, Coventry CV4 7AL, UK

[2]Department of Information Engineering, University of Florence, Florence I-50139, Italy

Abstract—By combining the work of J. R. Wait on a periodically loaded vertical wire grid and the work of D. A. Hill and J. R. Wait on a wire mesh, a novel generalized formulation, the Wait-Hill formulation, is obtained for the analysis of lumped-element periodically-loaded orthogonal wire grid generic frequency selective surfaces. The Wait-Hill formulation is simple and not restricted by the miniaturization assumption of current approximate simple methods for the analysis of loaded and unloaded wire grids. The results of the Wait-Hill formulation are shown to agree well with those of a commercial software.

1. INTRODUCTION

As the late professor Ben A. Munk emphasized in his books [1, 2] one has to avoid misconceptions when trying to realize novel frequency selective surface (FSS) configurations with improved properties. It is therefore necessary to derive formulations that can analyze FSS. The type of formulation depends on the unit cell configuration of the FSS which in turn depends on the specific application; periodic loading is employed for most popular FSS designs [1]. Our endeavor to gain insight into the behavior of periodically loaded FSS for achieving novel FSS designs of improved performance led us to consider establishing a generic configuration for FSS. We define generic FSS as the simplest combination of conductors and lumped elements characteristic of

Received 30 July 2013, Accepted 16 September 2013, Scheduled 25 October 2013

* Corresponding author: Christos Mias (c.mias@warwick.ac.uk).

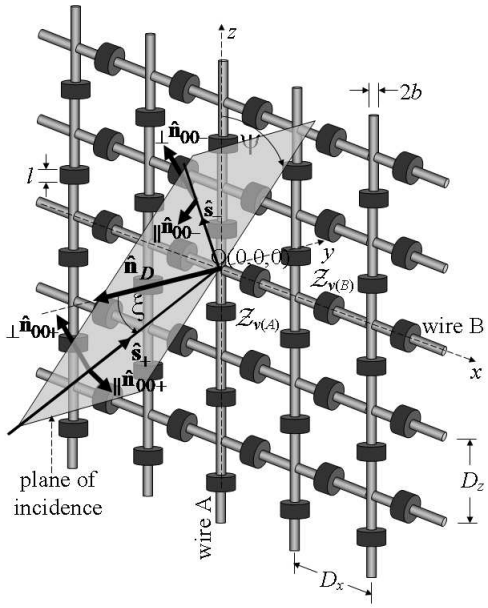

Figure 1. Geometry of the LE-PL-OWG generic FSS.

a whole class of periodically loaded FSS that includes bandstop, bandpass and multiband FSS. We must note that by lumped elements we mean electronic circuit networks of components, not just single R, L, C components. In FSS fabrication, the lumped elements may be of surface mount or printed form [1, 3, 4]. The lumped-element periodically-loaded orthogonal wire grid (LE-PL-OWG) FSS in Fig. 1 is a generic FSS. An example of a specific FSS that arises from this LE-PL-OWG generic FSS with capacitive loading is the well known Jerusalem cross [5].

This paper proposes a novel formulation that can provide theoretical and physical insight into the performance of the LE-PL-OWG bandstop FSS (generic bandpass FSS will be considered elsewhere). The formulation combines original work by J. R. Wait [6] on periodically loaded vertical wire grids and by D. A. Hill and J. R. Wait [7] on unloaded orthogonal wire grids. We name this generalized formulation the Wait-Hill (WH) formulation. Although the proposed WH formulation can be expressed in terms of the formalism in [6, 7], we choose, in this paper, to express it in terms of the formalism of B. A. Munk [1] as we found it convenient to use. Because of the equivalent radius approximation [1, 8], the analysis of narrow strip structures can practically be achieved through

the analysis of wire structures. Hence, we will only consider the analysis of LE-PL-OWG structures. The research to be presented is expected to be of interest in the field of theoretical analysis and applications of loaded wire grids [9–11] as it provides a formulation not restricted by the miniaturization assumption of the approximate methods in [10, 11]. The WH formulation is simple and provides insight on how the plane of incidence affects the current distribution in the LE-PL-OWG FSS. This insight cannot be obtained by the approximate methods in [10, 11]. It is to be noted that by assuming that the period is sufficiently electrically small, the WH formulation can provide approximate analytical expressions for the equivalent circuit impedance and scattering parameters of the LE-PL-OWG FSS for both perpendicular and parallel polarization that are independent of the plane of incidence. References [10, 11] also deal with equivalent circuit impedance approximate expressions which are obtained with a different approach. Differences between our approximate formulae and those of [10, 11] are discussed in Section 3 of the paper.

The paper is organized as follows. In Section 2, the generalized WH formulation is derived and its numerical results are compared with those of the commercial software CST [12]. In Section 3, it is shown how the WH formulation can provide theoretical and physical insight into the behavior of LE-PL-OWG bandstop FSS. In particular, the effect of the plane of incidence on the current harmonic amplitudes of the WH formulation is examined and simple approximate expressions for the FSS transmission coefficient are derived. The conclusions are drawn in Section 4.

2. DERIVATION OF THE GENERALIZED WAIT-HILL FORMULATION

The geometry of the periodic structure under analysis is shown in Fig. 1. The surrounding medium is assumed to be lossless with permittivity ε, permeability μ and intrinsic impedance η. A time dependence of the form of $e^{j\omega t}$ is assumed in the formulation and suppressed. The arbitrarily polarized electric field of the incident plane wave is decomposed into two components, one parallel and one perpendicular to the plane of incidence (see Fig. 1)

$$\mathbf{E}^{inc} = {}_{\parallel}E^{inc}(\mathbf{R})\,{}_{\parallel}\hat{\mathbf{n}}_{00+} + {}_{\perp}E^{inc}(\mathbf{R})\,{}_{\perp}\hat{\mathbf{n}}_{00+} \tag{1}$$

where [1],

$${}_{\parallel}\hat{\mathbf{n}}_{00\pm} = \frac{-\hat{\mathbf{x}}s_x s_y \pm \hat{\mathbf{y}}\left(s_x^2 + s_z^2\right) - \hat{\mathbf{z}}s_y s_z}{\sqrt{s_x^2 + s_z^2}}, \quad {}_{\perp}\hat{\mathbf{n}}_{00\pm} = \frac{-\hat{\mathbf{x}}s_z + \hat{\mathbf{z}}s_x}{\sqrt{s_x^2 + s_z^2}} \tag{2}$$

$$s_x = \sin\xi \sin\psi, \quad s_y = \cos\xi, \quad s_z = \sin\xi\cos\psi \tag{3}$$

with $\mathbf{R} = x\hat{\mathbf{x}} + y\hat{\mathbf{y}} + z\hat{\mathbf{z}}$. Subscript $\pm$ which refers to propagation in the $\pm y$ direction (Fig. 1) can be removed from ${}_{\perp}\hat{\mathbf{n}}_{00\pm}$. Because of the linearity of the problem, without loss of generality, it is assumed that the incident wave is either parallel or perpendicularly polarized and that

$${}_{\parallel}E^{inc}(\mathbf{R}) = {}_{\perp}E^{inc}(\mathbf{R}) = E_0 e^{-jk_r\hat{\mathbf{s}}\cdot\mathbf{R}} \tag{4}$$

where $k_r = 2\pi/\lambda$ and $\mathbf{s} = s_x\hat{\mathbf{x}} + s_y\hat{\mathbf{y}} + s_z\hat{\mathbf{z}}$.

For simplicity, the reference wire axes coincide with the z-axis for reference wire A ($x_A = 0$) and with the x-axis for reference wire B ($z_B = 0$). The origin O is at the intersection of the two wires, as shown in Fig. 1. It is also assumed that all wires have the same radius, b. Over the reference unit cell ($|x| \le D_x/2$, $|z| \le D_z/2$), the per unit length load impedance is

$$Z_{L(K)}(u) = \begin{cases} \mathcal{Z}_{v(K)}/l & \text{for} \quad (D_u - l)/2 \le |u| \le D_u/2 \\ 0 & \text{otherwise} \end{cases} \tag{5}$$

where $K = A$, $u = z$ for wire A and $K = B$, $u = x$ for wire B. $\mathcal{Z}_{v(K)}$ is the lumped element impedance (see Fig. 1). Since $Z_{L(K)}(u)$ is periodic,

$$Z_{L(K)}(u) = \sum_{n=-\infty}^{\infty} Z_{n(K)}\, e^{-j2\pi nu/D_u} \tag{6}$$

with $Z_{n(K)} = [(-1)^n(\mathcal{Z}_{v(K)}/D_u)\sin(n\pi l/D_u)]/(n\pi l/D_u)$.

The current flowing along the reference wires A and B is given by

$$I_K(u) = I_{\Pi(K)}(u)e^{-jk_r s_u u} \tag{7}$$

as $x_A = z_B = 0$. $I_{\Pi(K)}$ is the periodic part of the current function

$$I_{\Pi(K)}(u) = \sum_{p=-\infty}^{\infty} K_p e^{-j2\pi pu/D_u} \tag{8}$$

where $p = m$ for wire A and $p = q$ for wire B.

As indicated in [7] the scattered electric field $\mathbf{E}^{sc}$ can be derived from the magnetic vector potential. The wire boundary condition is [6],

$$\left({}_{\parallel,\perp}\mathbf{E}^{inc}\cdot\hat{\mathbf{u}} + \mathbf{E}^{sc}\cdot\hat{\mathbf{u}}\right)\Big|_{\mathbf{R}_b} = Z_{L(K)}(u)I_K(u) \tag{9}$$

where $\hat{\mathbf{u}} = \hat{\mathbf{z}}$, $\mathbf{R}_b = \mathbf{R}_b(0, b, z)$ for wire A and $\hat{\mathbf{u}} = \hat{\mathbf{x}}$, $\mathbf{R}_b = \mathbf{R}_b(x, b, 0)$ for wire B. From (9), following a procedure similar to [6, 7], the WH formulation is obtained,

$$\hat{Z}_{m(A)}A_m + {\sum_{n=-\infty}^{\infty}}' Z_{n(A)}A_{m-n} - \sum_{q=-\infty}^{\infty} C^{(m)}_{q(B)}B_q = \delta_{m0}E_0 e^{-jk_r s_y b}{}_{\parallel,\perp}n_{00z} \tag{10}$$

$$-\sum_{m=-\infty}^{\infty} C_{m(A)}^{(q)} A_m + \hat{Z}_{q(B)} B_q + \sum_{n=-\infty}^{\infty}{}' Z_{n(B)} B_{q-n}$$
$$= \delta_{0q} E_0 e^{-jk_r s_y b}{}_{\parallel,\perp} n_{00x} \tag{11}$$

where δ_{ij} is the Kronecker delta ($\delta_{ij} = 1$ for $i = j$ and $\delta_{ij} = 0$ for $i \neq j$), ${}_{\parallel,\perp} n_{00x}$ and ${}_{\parallel,\perp} n_{00z}$ are the x and z components respectively of the unit vectors of Equation (2), and

$$\hat{Z}_{m(A)} = \frac{j\omega\mu}{2D_x}\left(1-r_z^2\right)\left[-\frac{D_x}{\pi}\ln\left(1-e^{\frac{-2\pi b}{D_x}}\right)+\Delta_m+\frac{e^{-\Gamma_{m0}b}}{\Gamma_{m0}}\right]+Z_{0(A)} \tag{12}$$

$$\hat{Z}_{q(B)} = \frac{j\omega\mu}{2D_z}\left(1-r_x^2\right)\left[-\frac{D_z}{\pi}\ln\left(1-e^{\frac{-2\pi b}{D_z}}\right)+\Delta_q+\frac{e^{-\Gamma_{0q}b}}{\Gamma_{0q}}\right]+Z_{0(B)} \tag{13}$$

$$\Delta_m = \sum_{q=-\infty}^{\infty}{}' \left(\frac{e^{-\Gamma_{mq}b}}{\Gamma_{mq}} - \frac{e^{-\frac{2\pi}{D_x}|q|b}}{\frac{2\pi}{D_x}|q|}\right),$$

$$\Delta_q = \sum_{m=-\infty}^{\infty}{}' \left(\frac{e^{-\Gamma_{mq}b}}{\Gamma_{mq}} - \frac{e^{-\frac{2\pi}{D_z}|m|b}}{\frac{2\pi}{D_z}|m|}\right) \tag{14}$$

$$C_{q(B)}^{(m)} = \frac{j\omega\mu}{2D_z} r_z r_x \frac{e^{-\Gamma_{mq}b}}{\Gamma_{mq}} \tag{15}$$

$$C_{m(A)}^{(q)} = \frac{j\omega\mu}{2D_x} r_x r_z \frac{e^{-\Gamma_{mq}b}}{\Gamma_{mq}} \tag{16}$$

Throughout the paper, the symbol Σ' means that the index value of zero is excluded from the summation, i.e., in (14), the $q = 0$ term is omitted in Δ_m and the $m = 0$ term is omitted in Δ_q. Furthermore,

$$\Gamma_{mq} = jk_r r_y = jk_r\sqrt{1 - r_x^2 - r_z^2} \tag{17}$$

where $r_x = s_x + q\lambda/D_x$, $r_z = s_z + m\lambda/D_z$.

The range of m, q and n is suitably truncated to generate a set of simultaneous equations to be solved numerically. Here, $-Q \leq m \leq Q$ and $-Q \leq q \leq Q$. Solving for unknowns A_m and B_q means that for any value $m = h$ in (10) and $q = h$ in (11), the range of n is $-(Q-h) \leq n \leq (Q+h)$ in (10) and (11). The size of the final matrix is $(4Q+2)\times(4Q+2)$. As an example, (18) shows the matrix equation

assuming $Q = 1$,

$$\begin{bmatrix} Z_{-2(A)} & Z_{-1(A)} & \hat{Z}_{-1(A)} & -C^{(-1)}_{1(B)} & -C^{(-1)}_{0(B)} & -C^{(-1)}_{-1(B)} \\ Z_{-1(A)} & \hat{Z}_{0(A)} & Z_{1(A)} & -C^{(0)}_{1(B)} & -C^{(0)}_{0(B)} & -C^{(0)}_{-1(B)} \\ \hat{Z}_{1(A)} & Z_{1(A)} & Z_{2(A)} & -C^{(1)}_{1(B)} & -C^{(1)}_{0(B)} & -C^{(1)}_{-1(B)} \\ -C^{(-1)}_{1(A)} & -C^{(-1)}_{0(A)} & -C^{(-1)}_{-1(A)} & Z_{-2(B)} & Z_{-1(B)} & \hat{Z}_{-1(B)} \\ -C^{(0)}_{1(A)} & -C^{(0)}_{0(A)} & -C^{(0)}_{-1(A)} & Z_{-1(B)} & \hat{Z}_{0(B)} & Z_{1(B)} \\ -C^{(1)}_{1(A)} & -C^{(1)}_{0(A)} & -C^{(1)}_{-1(A)} & \hat{Z}_{1(B)} & Z_{1(B)} & Z_{2(B)} \end{bmatrix} \begin{bmatrix} A_1 \\ A_0 \\ A_{-1} \\ B_1 \\ B_0 \\ B_{-1} \end{bmatrix} = \begin{bmatrix} 0 \\ M_A \\ 0 \\ 0 \\ M_B \\ 0 \end{bmatrix} \tag{18}$$

where $M_A = E_0 \exp(-jk_r s_y b)_{\parallel,\perp} n_{00z}$ and $M_B = E_0 \exp(-jk_r s_y b)_{\parallel,\perp} n_{00x}$. Once the amplitude values A_m, B_q are computed, the scattered field at an observation point is obtained. Assuming that only the fundamental ($q = m = 0$) harmonic propagates, the co-polarized and cross-polarized transmission coefficients are given by

$$T_{w\,g} = \frac{{}_wE^{tran}(\mathbf{R}_{out})}{{}_gE^{inc}(\mathbf{R}_{in})} = \frac{E_0\delta_{wg} - F_{wg}}{E_0} e^{-j2k_r s_y y_{obs}} \tag{19}$$

where $\mathbf{R}_{out} = \mathbf{R}(x, y_{obs}, z)$, $\mathbf{R}_{in} = \mathbf{R}(x, -y_{obs}, z)$, δ_{wg} is the Kronecker delta, $g = \perp, \parallel$ and $w = \perp, \parallel$ represent the incident and scattered wave polarization, respectively, and

$$F_{wg} = \frac{\eta}{2D_x} ({}_gA_0) \frac{{}_wn_{00z}}{s_y} + \frac{\eta}{2D_z} ({}_gB_0) \frac{{}_wn_{00x}}{s_y} \tag{20}$$

In the Numerical Solution section, p. 357 of [7], Hill and Wait indicate that for parallel polarization and incidence along the wire axis ($\psi = 0°$) and near grazing (ξ near 90°) the convergence of the solution of their truncated matrix (Equation (18) with $Z_L = 0$) was extremely slow for their unloaded wire grid structure. The convergence difficulties were illustrated in Fig. 2 of [7]. By plotting the current distribution along the wires (shown in Fig. 3 of [7]), they found that the currents exhibited step discontinuities at the wire junction which satisfied Kirchhoff's current law (Equation (20) of [7]). As stated in [7], the primary reason for the slow convergence was the fact that the continuous expansion functions of the Fourier series in (8) are inefficient in synthesizing this discontinuous current at the wire junction. We also observed step discontinuities in the current plots of our FSS example (see FSS parameters in the caption of Fig. 2) obtained by solving (18). Based on the observed behavior of the higher order Fourier series coefficients of the currents in (8), Hill and Wait introduced a discontinuous periodic sawtooth function f_Δ in their current expressions in order to improve

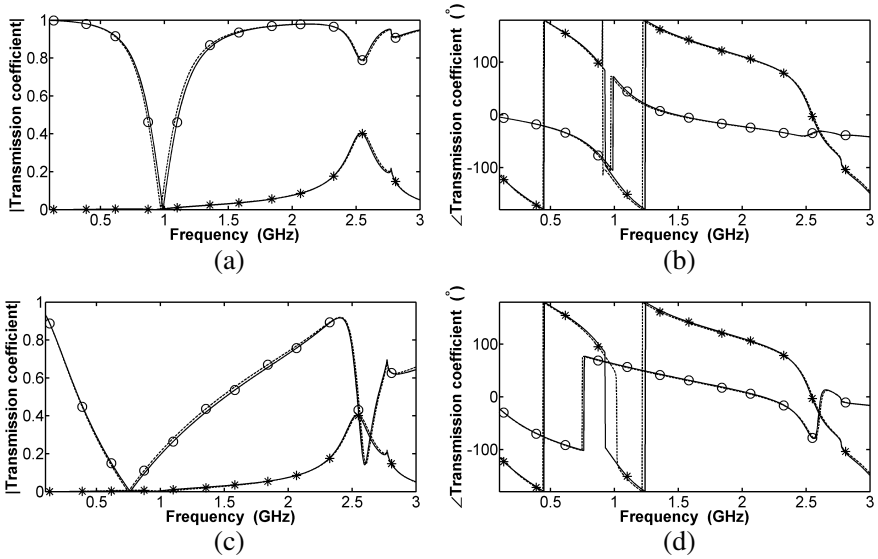

Figure 2. Co-polarized and cross-polarized transmission coefficient results for the LE-PL-OWG FSS with $\mathcal{Z}_{v(A)} = \mathcal{Z}_{v(B)} = 1/(j\omega C)$, $C = 1\,\text{pF}$, $l = 1.25\,\text{mm}$, $b = 0.36\,\text{mm}$, $D_x = D_z = 60\,\text{mm}$, $\xi = 70°$, $\psi = 22.5°$, $y_{obs} = 20\,\text{mm}$. The surrounding medium is free space. CST: Dashed line. WH method: Solid line. $Q = 10$, $Q' = 20 \times Q$, $Q_\Delta = 20 \times Q$. (a) Magnitude of $T_{\parallel\parallel}$: ($\circ$) and $T_{\perp\parallel}$: ($*$). (b) Phase of $T_{\parallel\parallel}$: ($\circ$) and $T_{\perp\parallel}$: ($*$). (c) Magnitude of $T_{\perp\perp}$: ($\circ$) and $T_{\parallel\perp}$: ($*$). (d) Phase of $T_{\perp\perp}$: ($\circ$) and $T_{\parallel\perp}$: ($*$).

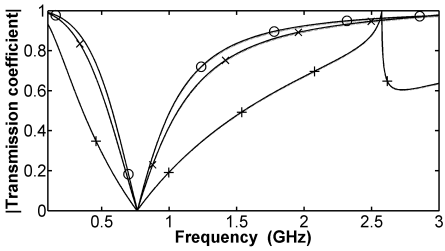

Figure 3. Co-polarized transmission coefficient magnitude $|T_{\perp\perp}|$. Solid line: WH method (LE-PL-OWG FSS). Dotted line: Wait's formulation (LE-PL vertical wire grid FSS). $\xi = 0°$, $\psi = 90°$ ($\circ$); $\xi = 35°$, $\psi = 90°$ ($\times$); $\xi = 70°$, $\psi = 90°$ ($+$). $\mathcal{Z}_{v(A)} = \mathcal{Z}_{v(B)} = 1/(j\omega C)$, $C = 1\,\text{pF}$, $l = 1.25\,\text{mm}$, $b = 0.36\,\text{mm}$, $D_x = D_z = 60\,\text{mm}$. The surrounding medium is free space.

the convergence of their results (see section on Improved Solution, pages 358–359 in [7]). Over the reference unit cell, the function f_Δ is defined as [7],

$$f_\Delta(u) = \Delta[U(u) - u/D_u - 1/2] = \sum_{p=-\infty}^{\infty}{}' \frac{j\Delta}{2\pi p} e^{-j2\pi pu/D_u}, \ \ |u| \leq D_u/2 \quad (21)$$

where $u = x$, z, $U(u)$ is the unit step function, and Δ is a complex unknown constant which represents the step of the function f_Δ at the wire junction.

For our FSS example, we observed that the higher order Fourier series coefficients of the currents in (8) closely follow the higher order Fourier series coefficients of the sawtooth function (21) when Δ is set equal to the current discontinuity jump at the wire junction. Hence, we also employ the Hill-Wait sawtooth function to improve the convergence of our results. Its implementation into the generalized WH formulation is shown below. Following [7], the $I_{\Pi(K)}$ in (8) can be expressed as

$$I_{\Pi(K)}(u) = \chi f_\Delta(u) + \sum_{p=-\infty}^{\infty} K'_p e^{-j2\pi pu/D_u} \quad (22)$$

where $\chi = 1$ for wire A and $\chi = -1$ for wire B. As in [7], based on (22), the current harmonic amplitudes K_p in (8) can be expressed in terms of the coefficients of the function f_Δ in (21) and the amplitudes K'_p as

$$K_p = j\chi\Delta(1 - \delta_{p0})/(2\pi p) + K'_p \quad (23)$$

Substituting (23) in (10) and (11) leads to

$$\begin{aligned} &\hat{Z}_{m(A)} A'_m + \sum_{n=-\infty}^{\infty}{}' Z_{n(A)} A'_{m-n} - \sum_{q=-\infty}^{\infty} C^{(m)}_{q(B)} B'_q + U_m\Delta \\ &= \delta_{m0} E_0 e^{-jk_r s_y b}{}_{\|,\perp} n_{00z} \quad (24) \\ &\quad - \sum_{m=-\infty}^{\infty} C^{(q)}_{m(A)} A'_m + \hat{Z}_{q(B)} B'_q + \sum_{n=-\infty}^{\infty}{}' Z_{n(B)} B'_{q-n} - V_q\Delta \\ &= \delta_{0q} E_0 e^{-jk_r s_y b}{}_{\|,\perp} n_{00x} \quad (25) \end{aligned}$$

respectively, where

$$\begin{aligned} U_m \ = \ & \hat{Z}_{m(A)} j\frac{(1 - \delta_{m0})}{2\pi m} + \sum_{n=-\infty}^{\infty}{}' Z_{n(A)} j\frac{(1 - \delta_{(m-n)0})}{2\pi(m-n)} \\ & + \sum_{q=-\infty}^{\infty} C^{(m)}_{q(B)} j\frac{(1 - \delta_{0q})}{2\pi q} \quad (26) \end{aligned}$$

and

$$V_q = \sum_{m=-\infty}^{\infty} C_{m(A)}^{(q)} j\frac{(1-\delta_{m0})}{2\pi m} + \hat{Z}_{q(B)} j\frac{(1-\delta_{0q})}{2\pi q} + \sum_{n=-\infty}^{\infty}{}' Z_{n(B)} j\frac{(1-\delta_{0(q-n)})}{2\pi(q-n)} \tag{27}$$

The extra equation needed because of the additional unknown complex parameter Δ is

$$\sum_{m=-\infty}^{\infty} G_{m(A)} A'_m - \sum_{q=-\infty}^{\infty} G_{q(B)} B'_q + W\Delta = 0 \tag{28}$$

where $G_{m(A)} = jk_r r_z$, $G_{q(B)} = jk_r r_x$ and $W = 1/D_x + 1/D_z$. As in [7], Equation (28) is obtained by substituting the current expression in (7), with $I_{\Pi(K)}$ given by (22), into Equation (26) of [7]. The latter equation, based on the parameters of Fig. 1, is re-written here for convenience as $\frac{1}{2}(\frac{\partial I_A}{\partial z}|_{z=0^-} + \frac{\partial I_A}{\partial z}|_{z=0^+}) = \frac{1}{2}(\frac{\partial I_B}{\partial x}|_{x=0^-} + \frac{\partial I_B}{\partial x}|_{x=0^+})$.

Equation (22) suggests that only the low order coefficients A'_m and B'_q need to be computed if the higher order current harmonic amplitudes of (8) are approximated well by the higher order coefficients of the function f_Δ in (21). Hence, in the computations, the range of m, q and n in the summations of (24) and (25) is suitably truncated to generate a set of simultaneous equations to be solved numerically. Here, $-Q \le m \le Q$ and $-Q \le q \le Q$. Solving for unknowns A'_m and B'_q means that for any value $m = h$ in (24) and $q = h$ in (25), the range of n is $-(Q-h) \le n \le (Q+h)$ in (24) and (25). The size of the final matrix is $(4Q+3) \times (4Q+3)$ because of the additional unknown Δ. As an example, (29) shows the matrix equation assuming $Q = 1$,

$$\begin{bmatrix}
Z_{-2(A)} & Z_{-1(A)} & \hat{Z}_{-1(A)} & -C_{1(B)}^{(-1)} & -C_{0(B)}^{(-1)} & -C_{-1(B)}^{(-1)} & U_{-1} \\
Z_{-1(A)} & \hat{Z}_{0(A)} & Z_{1(A)} & -C_{1(B)}^{(0)} & -C_{0(B)}^{(0)} & -C_{-1(B)}^{(0)} & U_0 \\
\hat{Z}_{1(A)} & Z_{1(A)} & Z_{2(A)} & -C_{1(B)}^{(1)} & -C_{0(B)}^{(1)} & -C_{-1(B)}^{(1)} & U_1 \\
-C_{1(A)}^{(-1)} & -C_{0(A)}^{(-1)} & -C_{-1(A)}^{(-1)} & Z_{-2(B)} & Z_{-1(B)} & \hat{Z}_{-1(B)} & -V_{-1} \\
-C_{1(A)}^{(0)} & -C_{0(A)}^{(0)} & -C_{-1(A)}^{(0)} & Z_{-1(B)} & \hat{Z}_{0(B)} & Z_{1(B)} & -V_0 \\
-C_{1(A)}^{(1)} & -C_{0(A)}^{(1)} & -C_{-1(A)}^{(1)} & \hat{Z}_{1(B)} & Z_{1(B)} & Z_{2(B)} & -V_1 \\
G_{1(A)} & G_{0(A)} & G_{-1(A)} & -G_{1(B)} & -G_{0(B)} & -G_{-1(B)} & W
\end{bmatrix}$$

$$\begin{bmatrix} A'_1 \\ A'_0 \\ A'_{-1} \\ B'_1 \\ B'_0 \\ B'_{-1} \\ \Delta \end{bmatrix} = \begin{bmatrix} 0 \\ M_A \\ 0 \\ 0 \\ M_B \\ 0 \\ 0 \end{bmatrix} \tag{29}$$

In the computations, the m, q summations in (14), which appear in the expressions of $\hat{Z}_{m(A)}$ and $\hat{Z}_{q(B)}$ of Equations (12) and (13), are truncated with truncation limit Q', such that in (14), $-Q' \leq m \leq Q'$ and $-Q' \leq q \leq Q'$.

Truncation is also applied to the m, q, n summations of Equations (26) and (27). In our code, for any value $m = h$ in (26) and $q = h$ in (27), the n summations of (26) and (27) have limits $-(Q_\Delta - h) \leq n \leq (Q_\Delta + h)$. Furthermore, for the q summation in (26) and the m summation in (27) the limits are $-Q_\Delta \leq q \leq Q_\Delta$ and $-Q_\Delta \leq m \leq Q_\Delta$, respectively. To examine the numerical convergence of the WH formulation, for various values of Q, Q' and Q_Δ, we consider as an example a LE-PL-OWG generic FSS (Fig. 1) periodically loaded with lumped element capacitors. The lumped element capacitance is $C = 1\,\text{pF}$, the lumped element length is $l = 1.25\,\text{mm}$, the wire radius is $b = 0.36\,\text{mm}$ and the period is $D_x = D_z = 60\,\text{mm}$. The incident plane wave is parallel polarized with incidence angles $\xi = 70^\circ$ and $\psi = 22.5^\circ$. The surrounding medium is free space. We found very good agreement among the co-polarized and cross-polarized transmission coefficient magnitude results of the following truncation limits: (i) $Q = 5$, $Q' = 40 \times Q$, $Q_\Delta = 40 \times Q$; (ii) $Q = 10$, $Q' = 20 \times Q$, $Q_\Delta = 20 \times Q$; (iii) $Q = 40$, $Q' = 40 \times Q$, $Q_\Delta = 40 \times Q$. Based on these results we use the values $Q = 10$, $Q' = 20 \times Q$ and $Q_\Delta = 20 \times Q$ in the simulations that follow for this FSS example. Fig. 2 shows that for our FSS example there is a very good agreement between the WH formulation results and the CST results.

3. WAIT-HILL FORMULATION ANALYSIS OF GENERIC FSS

This section considers how the WH formulation provides insight into the behavior of LE-PL OWG generic FSS. Different planes of incidence are considered. We assume that $D_x = D_z = D$ and $Z_{n(A)} = Z_{n(B)} = Z_n$ as this is often the case in FSS configurations with orthogonal axes

of periodicity [1]. To aid the analysis that follows, we rewrite (11) as

$$\hat{Z}_{q(B)}B_q + \sum_{n=-\infty}^{\infty}{}' Z_n B_{q-n} = R^{(q)} \tag{30}$$

where $R^{(q)} = \delta_{0q}E_0 e^{-jk_r s_y b}{}_{\parallel,\perp}n_{00x} + \sum_{m=-\infty}^{\infty} C^{(q)}_{m(A)}A_m$.

Hence we can write the following matrix equation

$$\begin{bmatrix} \ddots & \vdots & \vdots & \vdots & \vdots & \vdots & \iddots \\ \cdots & Z_{-4} & Z_{-3} & Z_{-2} & Z_{-1} & \hat{Z}_{-2(B)} & \cdots \\ \cdots & Z_{-3} & Z_{-2} & Z_{-1} & \hat{Z}_{-1(B)} & Z_1 & \cdots \\ \cdots & Z_{-2} & Z_{-1} & \hat{Z}_{0(B)} & Z_1 & Z_2 & \cdots \\ \cdots & Z_{-1} & \hat{Z}_{1(B)} & Z_1 & Z_2 & Z_3 & \cdots \\ \cdots & \hat{Z}_{2(B)} & Z_1 & Z_2 & Z_3 & Z_4 & \cdots \\ \iddots & \vdots & \vdots & \vdots & \vdots & \vdots & \ddots \end{bmatrix} \begin{bmatrix} \vdots \\ B_2 \\ B_1 \\ B_0 \\ B_{-1} \\ B_{-2} \\ \vdots \end{bmatrix} = \begin{bmatrix} \vdots \\ R^{(-2)} \\ R^{(-1)} \\ R^{(0)} \\ R^{(1)} \\ R^{(2)} \\ \vdots \end{bmatrix} \tag{31}$$

3.1. Perpendicular Polarization with $\psi = 90°$ ($s_z = 0$)

Since $s_z = 0$ it follows that

$$C^{(q)}_{m(A)} = \frac{j\omega\mu}{2D} r_x \frac{m\lambda}{D} \frac{e^{-\Gamma_{mq}b}}{\Gamma_{mq}}, \quad C^{(q)}_{0(A)} = 0, \quad C^{(q)}_{|m|(A)} = -C^{(q)}_{-|m|(A)} \tag{32}$$

It is also to be noted that ${}_{\perp}n_{00x} = 0$. Since the loading and the unit cell are symmetric (about the x-axis) along the z-direction, then for the incidence considered we expect $A_m = A_{-m}$ and therefore $R^{(q)} = 0$ for every q. Since the right hand side (RHS) vector of (31) is zero, and assuming the matrix can be inverted, one obtains $B_q = 0$ for every q. Numerical results confirm the above current harmonic amplitude relations ($A_m = A_{-m}$ and $B_q = 0$). From (19), the cross-polarization transmission coefficient $T_{\parallel\perp}$ is zero for any angle of incidence ξ since ${}_{\parallel}n_{00z} = 0$ and ${}_{\perp}B_0 = 0$. This was anticipated because of the structure's symmetry [13].

Since $B_q = 0$, the LE-PL-OWG FSS formulation (18) reduces to that of plane wave scattering from a LE-PL vertical wire grid FSS which was considered in [6]. Fig. 3 demonstrates this fact by comparing the WH formulation (LE-PL-OWG FSS) results with those of the Wait's formulation (LE-PL vertical wire grid FSS) [6].

3.2. Parallel Polarization with $\psi = 0^\circ$ ($s_x = 0$)

Since $s_x = 0$, it follows from (16) that

$$C_{m(A)}^{(q)} = \frac{j\omega\mu}{2D}\frac{q\lambda}{D} r_z \frac{e^{-\Gamma_{mq}b}}{\Gamma_{mq}} \tag{33}$$

and ${}_{\parallel}n_{00x} = 0$. Therefore, $R^{(0)} = 0$ and (for $q \neq 0$)

$$R^{(q)} = \sum_{m=-\infty}^{\infty} C_{m(A)}^{(q)} A_m = -\sum_{m=-\infty}^{\infty} C_{m(A)}^{(-q)} A_m = -R^{(-q)} \tag{34}$$

In addition, from (13), $\hat{Z}_{q(B)} = \hat{Z}_{-q(B)}$. Since the wire B has lumped element loading that is symmetric about the point of intersection with wire A then $Z_n = Z_{-n}$. Hence substituting $R^{(-q)} = -R^{(q)}$, $Z_{-n} = Z_n$ and $\hat{Z}_{-q(B)} = \hat{Z}_{q(B)}$ in the matrix of (31) leads to a bisymmetric matrix. Its inverse is also bisymmetric. Therefore assuming that the middle row of the inverse matrix is, say, $[\ldots\ a\ b\ c\ b\ a\ldots]$ then $B_0 = 0$. Furthermore, $B_q = -B_{-q}$ due to the form of the RHS vector and the bisymmetry of the inverse matrix. Thus, the current $I_B(x)$ is an odd function. Numerical results confirm the above current harmonic amplitude relations ($B_0 = 0$ and $B_q = -B_{-q}$). From (19), the cross-polarization transmission coefficient $T_{\perp\parallel}$ is zero for any angle of incidence ξ since ${}_{\perp}n_{00z} = 0$ and ${}_{\parallel}B_0 = 0$. This was expected because of the structure's symmetry [13].

Because of the presence of the induced current $I_B(x)$ one anticipates that the transmission coefficient from the LE-PL-OWG FSS will be different from that of the LE-PL vertical wire grid FSS [6]. This is confirmed in Fig. 4. Fig. 4 shows that there is a deviation of the resonance frequency with the angle of incidence ξ. However this deviation is smaller for the OWG FSS than for the vertical wire grid FSS. To obtain more insight for our FSS example, by simplifying (29), we found it useful to employ a crude approximation, i.e., we assume that (22) can be expressed as (ignoring, for the moment, the particular plane of incidence and the fact that $B_0 = 0$)

$$I_{\Pi(K)}(u) \approx K_0 + \chi f_\Delta(u) \tag{35}$$

Then, from (35) and the fact that $B_0 = 0$, (29) reduces to

$$\begin{bmatrix} \hat{Z}_{0(A)} & U_0 \\ G_{0(A)} & W \end{bmatrix} \begin{bmatrix} A_0 \\ \Delta \end{bmatrix} = \begin{bmatrix} E_0\ {}_{\parallel,\perp}n_{00z} \\ 0 \end{bmatrix} \tag{36}$$

where we have assumed that $\exp(-jk_r s_y b) \approx 1$. From its solution we obtain,

$$A_0 = \frac{W E_{0\parallel,\perp} n_{00z}}{\hat{Z}_{0(A)} W - G_{0(A)} U_0} \tag{37}$$

Substituting the amplitude approximation (37) in Equation (19) yields the parallel polarization transmission coefficient expression that will be developed in Section 3.4, Equation (50), in which $_{\parallel}\mathcal{Z}_g$ is given by

$$\begin{aligned} {}_{\parallel}\mathcal{Z}_g &= \left[-\frac{j\omega\mu D}{2\pi}\left(1-s_z^2\right)\ln\left(1-e^{\frac{-2\pi b}{D}}\right)+\mathcal{Z}_v\right] \\ &\quad +\left[-\frac{j\omega\mu D}{4\pi}s_z^2\ln\left(1-e^{\frac{-2\pi b}{D}}\right)\right] \\ &= \left\{-\frac{j\omega\mu D}{4\pi}(2-\sin^2\xi)\ln\left(1-e^{\frac{-2\pi b}{D}}\right)\right\}+\mathcal{Z}_v \end{aligned} \tag{38}$$

since $s_z = \sin\xi$. Results from (50) are plotted in Fig. 4. In obtaining (38), we assumed that D/λ is sufficiently small so that we can neglect the term Δ_0 in $\hat{Z}_{0(A)}$. The parameter $_{\parallel}\mathcal{Z}_g$ represents the transmission line equivalent circuit impedance of the LE-PL-OWG FSS for the present plane of incidence. The transmission line characteristic impedance is ηs_y. The square bracket term in the first line of (38) is the transmission line equivalent circuit impedance of the isolated LE-PL vertical wire grid FSS [6], and it is the sum of the impedance of the vertical wire grid inductance and the impedance of the lumped element capacitive load. The square bracket term in the second line of (38) is the impedance of an additional inductance due to the presence of the horizontal wires; this inductance increases as the angle of incidence ξ increases. At the resonance frequency, $_{\parallel}\mathcal{Z}_g = 0$. It is thus explained,

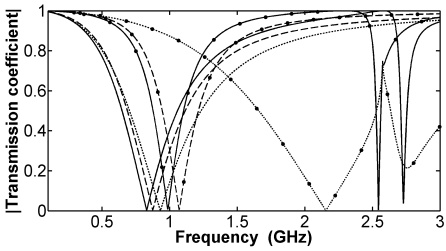

Figure 4. Co-polarized transmission coefficient magnitude $|T_{\parallel\parallel}|$. Solid line: WH method (LE-PL-OWG FSS). Dotted line: Wait's formulation [6] (LE-PL vertical wire grid FSS). Dashed line: Eqs. (50) with (38). For the solid, dotted and dashed lines with no symbols the incidence angles are $\xi = 35°$ and $\psi = 0°$. For the solid, dotted and dashed lines with symbol (•) the incidence angles are $\xi = 70°$ and $\psi = 0°$. $\mathcal{Z}_{v(A)} = \mathcal{Z}_{v(B)} = 1/(j\omega C)$, $C = 1\,\text{pF}$, $l = 1.25\,\text{mm}$, $b = 0.36\,\text{mm}$, $D_x = D_z = 60\,\text{mm}$. The surrounding medium is free space.

for the first time, why the deviation in the resonance frequency of the LE-PL-OWG FSS is less than that of the LE-PL vertical wire grid FSS of [6] as the angle of incidence ξ increases. As will be shown, elsewhere, for lumped element periodically loaded vertical wire grids, the resonance frequency deviation can be reduced by employing a lumped element inductance. For LE-PL-OWG FSS, we demonstrate this in Section 3.4 where we consider an arbitrary angle of incidence.

For periodically loaded FSS, it is noted that an approximate formulation for the Jerusalem cross FSS impedance was proposed in [10] (see Equation (13) of [10] and Equations (A7) and (A9) of [14]) but its inductive term corresponds to that of the first square bracket term of the first line in (38), i.e., it does not take into consideration the presence of the horizontal wires. For the unloaded planar mesh, the curly bracket term in the second line of (38) was obtained in [11] (see Equation (5) in [11]) from the average boundary condition of Equation (1) of [11]. As we do for (38), the authors of [11] obtained their Equation (5) for a given direction of incidence (see paragraph above Equation (5) in [11]). However, using the WH formulation approach, we will show in Section 3.4 that the approximate impedance expression in the curly brackets is valid for any arbitrary plane of incidence, see our Equation (51).

3.3. Incidence for $\psi = 45°$ ($s_x = s_z$)

Since our example is diagonally symmetric, i.e., $D_x = D_z = D$ and $Z_{n(A)} = Z_{n(B)}$, then $\hat{Z}_{m(A)} = \hat{Z}_{q(B)}$ for any $m = q$. Also, $C^{(q)}_{m(A)} = C^{(m)}_{q(B)}$ for any $m = q$. Therefore, (18) can be written as follows

$$\begin{bmatrix} \mathbf{Z} & -\mathbf{C} \\ -\mathbf{C} & \mathbf{Z} \end{bmatrix} \begin{bmatrix} \mathbf{A} \\ \mathbf{B} \end{bmatrix} = \begin{bmatrix} \mathbf{E}_{\parallel,\perp} n_{00z} \\ \mathbf{E}_{\parallel,\perp} n_{00x} \end{bmatrix} \tag{39}$$

Equation (39) is solved for each polarization. For perpendicular polarization, ${}_{\perp}n_{00z} = 1/\sqrt{2}$ and ${}_{\perp}n_{00x} = -1/\sqrt{2}$. Hence (39) leads to $\mathbf{A} = -\mathbf{B}$. Therefore $A_0 = -B_0$. For parallel polarization ${}_{\parallel}n_{00x} = {}_{\parallel}n_{00z} = -s_y/\sqrt{2}$ and (39) leads to $\mathbf{A} = \mathbf{B}$. Therefore $A_0 = B_0$. Numerical results confirm the above current harmonic amplitude relations. Substituting these relations into the transmission coefficient (19) results in $T_{\parallel\perp} = T_{\perp\parallel} = 0$ for any angle of incidence ξ. The absence of cross-polarization, for both polarizations, is numerically confirmed in Fig. 5 where co-polarization and cross-polarization transmission coefficient magnitude results are shown for $\xi = 70°$.

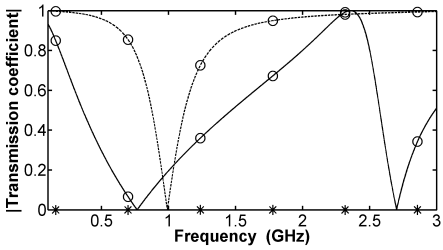

Figure 5. Co-polarized and cross-polarized transmission coefficient magnitude results (WH method) for $\xi = 70°$, $\psi = 45°$. $|T_{\perp\perp}|$: solid line with ($\circ$); $|T_{\parallel\parallel}|$: dashed line with ($\circ$); $|T_{\parallel\perp}|$: solid line with ($*$); $|T_{\perp\parallel}|$: dashed line with ($*$). $\mathcal{Z}_{v(A)} = \mathcal{Z}_{v(B)} = 1/(j\omega C)$, $C = 1\,\text{pF}$, $l = 1.25\,\text{mm}$, $b = 0.36\,\text{mm}$, $D_x = D_z = 60\,\text{mm}$. The surrounding medium is free space.

3.4. Incidence at an Arbitrary Angle

In Fig. 2, we observe that the cross-polarization transmission coefficients of the two polarizations are equal. This is anticipated from the theoretical work of Li [15] on the symmetries of cross-polarization diffraction coefficients of gratings which is based on the reciprocity theorem [16]. The WH formulation can provide a mathematical confirmation of this fact for our LE-PL-OWG generic FSS as follows. Equation (18) can be written as (each of the submatrices has a size $(2Q+1) \times (2Q+1)$)

$$\begin{bmatrix} \mathbf{Z}_{(A)} & -\mathbf{C}_{(B)} \\ -\mathbf{C}_{(A)} & \mathbf{Z}_{(B)} \end{bmatrix} \begin{bmatrix} \mathbf{A} \\ \mathbf{B} \end{bmatrix} = \begin{bmatrix} \mathbf{E}_{\parallel,\perp} n_{00z} \\ \mathbf{E}_{\parallel,\perp} n_{00x} \end{bmatrix} \tag{40}$$

where $\mathbf{Z}_{(A)}$ and $\mathbf{Z}_{(B)}$ are persymmetric. Since $D_x = D_z = D$, $\mathbf{C}_{(A)}$ and $\mathbf{C}_{(B)}$ have the same antidiagonal and mirror each other about the antidiagonal. From (40) one obtains, through matrix inversion, that

$$\begin{bmatrix} \mathbf{A} \\ \mathbf{B} \end{bmatrix} = \begin{bmatrix} \mathbf{\Theta} & \mathbf{\Lambda} \\ \mathbf{\Phi} & \mathbf{\Psi} \end{bmatrix} \begin{bmatrix} \mathbf{E}_{\parallel,\perp} n_{00z} \\ \mathbf{E}_{\parallel,\perp} n_{00x} \end{bmatrix} \tag{41}$$

We found numerically that the submatrices of the inverse matrix have the same properties as the submatrices of the matrix of (40), i.e., $\mathbf{\Theta}$ and $\mathbf{\Psi}$ are persymmetric and $\mathbf{\Lambda}$ and $\mathbf{\Phi}$ have the same antidiagonal and mirror each other about the antidiagonal. Obtaining from (41) expressions for A_0 and B_0 and substituting these in (20) yields

$$\begin{aligned} F_{wg} \;=\; & \frac{\eta E_0 e^{-jk_r s_y b}}{2Ds_y} \times [\Theta_{Q+1,Q+1}\, {}_g n_{00z}\, {}_w n_{00z} + \Lambda_{Q+1,Q+1}\, {}_g n_{00x}\, {}_w n_{00z} \\ & + \Phi_{Q+1,Q+1}\, {}_g n_{00z}\, {}_w n_{00x} + \Psi_{Q+1,Q+1}\, {}_g n_{00x}\, {}_w n_{00x}] \end{aligned} \tag{42}$$

Because of the relation of $\mathbf{\Lambda}$ and $\mathbf{\Phi}$ it follows that $\Lambda_{Q+1,Q+1} = \Phi_{Q+1,Q+1}$. Hence, $F_{\parallel\perp} = F_{\perp\parallel}$ and, from (19), $T_{\parallel\perp} = T_{\perp\parallel}$.

Assuming that the period is electrically small, as the period used in the FSS example of Fig. 7, we again consider the crude approximation (35) based on which (29) reduces to

$$\begin{bmatrix} \hat{Z}_{0(A)} & -C^{(0)}_{0(B)} & U_0 \\ -C^{(0)}_{0(A)} & \hat{Z}_{0(B)} & -V \\ G_{0(A)} & -G_{0(B)} & W \end{bmatrix} \begin{bmatrix} A_0 \\ B_0 \\ \Delta \end{bmatrix} = \begin{bmatrix} E_{0\ \parallel,\perp} n_{00z} \\ E_{0\ \parallel,\perp} n_{00x} \\ 0 \end{bmatrix} \tag{43}$$

where we have assumed that $\exp(-jk_r s_y b) \approx 1$. Assuming also that λ/D is sufficiently large for Δ_0 to be neglected and for the approximations $s_x + \lambda q/D \approx \lambda q/D$ and $s_z + \lambda m/D \approx \lambda m/D$ to hold for $q \neq 0$ and $m \neq 0$, we obtain from (12), (13), (15), (16), (26) and (27) the following expressions,

$$\hat{Z}_{0(A)} \approx (1 - s_z^2)X + (1 - s_z^2)\frac{\eta}{2Ds_y} + Z_0 \tag{44}$$

$$\hat{Z}_{0(B)} \approx \left(1 - s_x^2\right)X + \left(1 - s_x^2\right)\frac{\eta}{2Ds_y} + Z_0 \tag{45}$$

$$C^{(0)}_{0(A)} = C^{(0)}_{0(B)} \approx s_x s_z \frac{\eta}{2Ds_y} \tag{46}$$

$$U_0 \approx j\frac{\lambda}{2\pi D} s_z X \text{ and } V_0 \approx j\frac{\lambda}{2\pi D} s_x X \tag{47}$$

where $X = -\frac{j\omega\mu}{2\pi}\ln(1 - e^{\frac{-2\pi b}{D}})$.

Solving (43) and substituting the expressions for A_0 and B_0 in (19) we obtain the following expressions for the co-polarized transmission coefficients

$$T_{\perp\perp} = \left(1 - \frac{\eta/(2s_y)}{\eta/(2s_y) + {}_\perp\mathcal{Z}_g}\right) e^{-j2k_r s_y y_{obs}} \tag{48}$$

where

$${}_\perp\mathcal{Z}_g = DX + \mathcal{Z}_v \tag{49}$$

and

$$T_{\parallel\parallel} = \left(1 - \frac{\eta s_y/2}{\eta s_y/2 + {}_\parallel\mathcal{Z}_g}\right) e^{-j2k_r s_y y_{obs}} \tag{50}$$

where

$${}_\parallel\mathcal{Z}_g = (1 + s_y^2)DX/2 + \mathcal{Z}_v \tag{51}$$

with $s_y = \cos\xi$. Furthermore, for the cross-polarized transmission coefficients,

$$T_{\parallel\perp} = T_{\perp\parallel} = 0 \tag{52}$$

For both incident polarizations, expressions for Δ in (43) indicate that its value is small for small D and large λ.

In Equations (48)–(51), the transmission coefficients and the bandstop resonance frequencies (at which ${}_{\perp}\mathcal{Z}_g$ and ${}_{\parallel}\mathcal{Z}_g$ are zero) are independent of the azimuthal angle ψ. However, the transmission coefficients in Equations (48) and (50) are dependent on the angle of incidence ξ. In addition, Equation (49) indicates that the resonance frequency for perpendicular polarization is independent of ξ, while Equation (51) indicates that the resonance frequency for parallel polarization changes as ξ changes. As it will be shown, elsewhere, for a LE-PL vertical wire grid FSS, this deviation of the parallel polarization resonance frequency can be reduced by adding in our LE-PL-OWG generic bandstop FSS, in series with the lumped element capacitance, a lumped element inductance. If this inductance value is such that the X terms in (49), (51) can be neglected, then (48), (50) are simplified further as follows

$$T_{\perp\perp} = \left[1 - \frac{\eta/(2s_y)}{\eta/(2s_y) + \mathcal{Z}_v}\right] e^{-j2k_r s_y y_{obs}} \tag{53}$$

$$T_{\parallel\parallel} = \left[1 - \frac{\eta s_y/2}{\eta s_y/2 + \mathcal{Z}_v}\right] e^{-j2k_r s_y y_{obs}} \tag{54}$$

In Equations (53) and (54), the resonance frequency is the same for both polarizations and independent of ξ. However, the transmission coefficients of (53) and (54) are still dependent on the angle of incidence ξ.

We now demonstrate the above approximations using a new FSS example. This new LE-PL-OWG bandstop FSS is obtained from the FSS of Fig. 2 by reducing the period D of the FSS of Fig. 2 to $D^{(\text{new})} = 10\,\text{mm}$. Reducing the period reduces $X$to $X^{(\text{new})}$. To maintain the

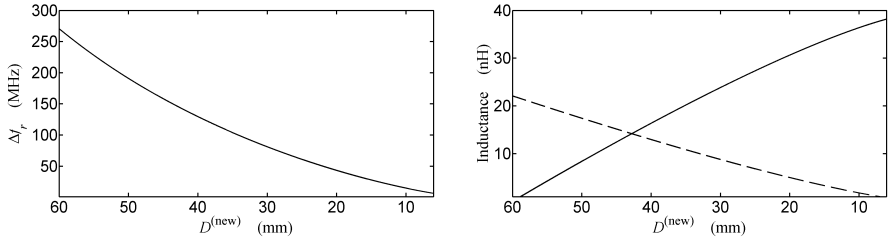

Figure 6. (a) The parallel polarization resonance frequency deviation, Δf_r, and (b) inductance values, L (solid line) and $L_w^{(\text{new})}(\xi)$ (dashed line), versus the new period $D^{(\text{new})}$. $b = 0.36\,\text{mm}$, $C = 1\,\text{pF}$, $\xi = 70°$.

resonance frequency at a similar value (at normal incidence) to that of the FSS of Fig. 2 we add (following simulations) a lumped element inductance of value $L = 40\,\text{nH}$ in series with the lumped element capacitance, i.e., $\mathcal{Z}_v = 1/(j\omega C) + j\omega L$. To justify the choice of the period $D^{(\text{new})}$ and the lumped element inductance value, we make use of (51) since we have shown in Fig. 4 that (38) approximates satisfactorily the FSS behaviour. Let $j\omega L_w(\xi) = (1 + s_y^2)DX/2$ where $L_w(\xi)$ is, according to (51), the parallel polarization wire inductance at angle ξ of the FSS of Fig. 4. Let also $j\omega L_w^{(\text{new})}(\xi) = (1+s_y^2)D^{(\text{new})}X^{(\text{new})}/2$ where $L_w^{(\text{new})}(\xi)$ is the parallel polarization wire inductance at angle ξ of the new FSS. Hence, in order for the two FSS configurations to have, at normal incidence, the same resonance frequency, a lumped element inductance L must be added to the new FSS of value $L = L_w(0) - L_w^{(\text{new})}(0)$. If, for the new FSS, the parallel polarization resonance frequency at normal incidence is $f_r(0)$ and at angular incidence is $f_r(\xi)$ then the resonance frequency deviation is, according to (51),

$$\Delta f_r = f_r(\xi) - f_r(0) = \left\{2\pi\sqrt{\left[L_w^{(\text{new})}(\xi)+L\right]C}\right\}^{-1} - \left\{2\pi\sqrt{L_w(0)C}\right\}^{-1} \quad (55)$$

A plot of Δf_r, L, $L_w^{(\text{new})}(\xi)$ is shown in Fig. 6 for $\xi = 70°$. To have a

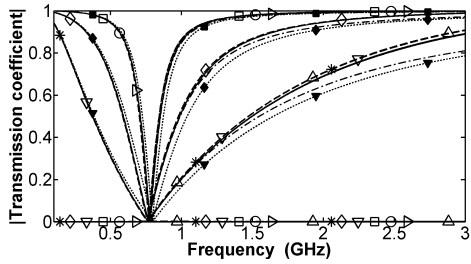

Figure 7. Transmission coefficient magnitude results. $D_x = D_z = 10\,\text{mm}$, $l = 1.25\,\text{mm}$, $b = 0.36\,\text{mm}$, $\mathcal{Z}_v = 1/(j\omega C) + j\omega L$, $C = 1\,\text{pF}$, $L = 40\,\text{nH}$. Dashed line (unfilled symbols): CST. Solid line: WH method. Dash-dot line: (48) and (50). Dotted line (filled symbols): (53) and (54). Normal incidence: ($\Diamond$). $|T_{\perp\perp}|$, $|T_{\parallel\perp}|$, $\xi = 70°$: $\psi = 22.5°$ ($*$); $\psi = 45°$ ($\triangle$); $\psi = 90°$ ($\triangledown$). $|T_{\parallel\parallel}|$, $|T_{\perp\parallel}|$, $\xi = 70°$: $\psi = 0°$ ($\square$); $\psi = 22.5°$ ($\circ$); $\psi = 45°$ ($\triangleright$). For clarity unfilled symbols are used on CST curves only since the curves of the WH method and Eqs. (48) and (50) closely follow the CST results. The surrounding medium is free space.

parallel polarization resonance frequency deviation of around 15 MHz we choose $D^{(\text{new})} = 10\,\text{mm}$. The required lumped element inductance is 36 nH (approx.) which is close to the numerically chosen value of 40 nH. $L_w^{(\text{new})}(\xi)$ is about 1.8 nH.

Figure 7 shows co-polarized and cross-polarized transmission coefficient magnitude results obtained from: (i) Eqs. (53) and (54); (ii) the WH formulation with $Q = 2$, $Q' = 100 \times Q$, $Q_\Delta = 100 \times Q$; (iii) Eqs. (48) and (50); and (iv) CST. We observe a good agreement among them; the frequency span of the resonance frequencies of all the curves does not exceed 50 MHz. This good agreement indicates that our choice of FSS parameters is consistent with the assumptions made to obtain (48), (50) and (53), (54).

4. CONCLUSION

The generalized Wait-Hill formulation was created by synthesizing the work of J. R. Wait on a periodically loaded vertical wire grid and the work of D. A. Hill and J. R. Wait on a wire mesh. For the considered examples, the obtained numerical results were shown to agree well with a commercial software. The capability of the Wait-Hill formulation to analyze LE-PL-OWG generic bandstop FSS was also highlighted. We thus expect that the Wait-Hill formulation will be useful to the FSS community. We also believe that this paper will be of interest to those working with connected array antennas. Future work will deal with the magnetic current version of the Wait-Hill formulation for the analysis of lumped element periodically loaded orthogonal narrow slot bandpass FSS and the design of novel FSS.

REFERENCES

1. Munk, B. A., *Frequency Selective Surfaces: Theory and Design*, John Wiley and Sons, 2000.
2. Munk, B. A., *Finite Arrays and FSS*, John Wiley and Sons, 2003.
3. Mias, C., "Frequency selective surfaces loaded with surface-mount reactive components," *Electronics Letters*, Vol. 39, No. 9, 724–726, 2003.
4. Li, M. and N. Behdad, "A third-order bandpass frequency selective surface with a tunable transmission null," *IEEE Trans. Antennas Propagat.*, Vol. 60, No. 4, 2109–2113, 2012.
5. Anderson, I., "On the theory of self resonant grids," *The Bell System Technical Journal*, Vol. 54, No. 4, 1725–1731, 1975.

6. Wait, J. R., "Theory of scattering from a periodically loaded wire grid," *IEEE Trans. Antennas Propagat.*, Vol. 25, No. 3, 409–413, 1977.
7. Hill, D. A. and J. R. Wait, "Electromagnetic scattering of an arbitrary plane-wave by a wire mesh with bonded junctions," *Canadian Journal of Physics*, Vol. 54, No. 4, 353–361, 1976.
8. Butler, C., "The equivalent radius of a narrow conducting strip," *IEEE Trans. Antennas Propag.*, Vol. 30, No. 4, 755–758, Jul. 1982.
9. Iigusa, K., H. Harada, S. Kato, J. Hirokawa, and M. Ando, "Periodically loaded straight wires for radio wave transmission control," *IEEE Trans. Antennas Propag.*, Vol. 59, No. 1, 328–332, 2011.
10. Simovski, C. R., P. de Maagt, and I. V. Melchakova, "High-impedance surfaces having stable resonance with respect to polarization and incidence angle," *IEEE Trans. Antennas Propag.*, Vol. 53, No. 3, 908–914, 2005.
11. Luukkonen, O., C. Simovski, G. Granet, G. Goussetis, D. Lioubtchenko, A. V. Raisanen, and S. A. Tretyakov, "Simple and accurate analytical model of planar grids and high-impedance surfaces comprising metal strips or patches," *IEEE Trans. Antennas Propag.*, Vol. 56, No. 6, 1624–1632, 2008.
12. CST 2012, Computer Simulation Technology, Darmstadt, Germany, www.cst.com.
13. Luebbers, R. J. and B. A. Munk, "Cross polarization losses in periodic arrays of loaded slots," *IEEE Trans. Antennas Propag.*, Vol. 23, No. 2, 159–164, 1975.
14. Padooru, Y. R., A. B. Yakovlev, P.-Y. Chen, and A. Alu, "Analytical modeling of conformal mantle cloaks for cylindrical objects using sub-wavelength printed and slotted arrays," *J. Appl. Phys.*, Vol. 112, 034907, 2012.
15. Li, L., "Symmetries of cross-polarization diffraction coefficients of gratings," *Journal of the Optical Society of America A — Optics Image Science and Vision*, Vol. 17, No. 5, 881–887, May 2000.
16. Vincent, P. and M. Neviere, "The reciprocity theorem for corrugated surfaces used in conical diffraction mountings," *Optica Acta*, Vol. 26, No. 7, 889–898, 1979.